Macromolecular Research, Vol. 12, No. 2, pp 178-188 (2004)

Evaluation of Internal Structure and Morphology of Poly(benzyl ether) Dendrimers by Molecular Dynamics Simulations

Taewan Hong and Hyung-Il Kim*

Department of Fine Chemicals Engineering and Chemistry, Chungnam National University, Daejeon 305-764, Korea

Received July 2, 2003; Revised February 20, 2004

Abstract: We performed molecular dynamics (MD) simulations at 300 K on a series of poly(benzyl ether) (PBE) dendrimers having a different core functionalities. We used the rotational isomeric state Metropolis Monte Carlo (RMMC) method to construct the initial configuration in a periodic boundary cell (PBC) before the MD simulations were undertaken. To elucidate the effects that the structural features have on the chain dimension, the overall internal structure, and the morphology, we monitored the radii of gyration, R_g, and the conformational changes during the simulations. The PBE dendrimers in a glassy state adopted less-extended structures when compared with the conformations obtained from the RMMC calculations. We found that R_g of the PBE dendrimer depends on the molecular weight, M, according to the relation, $R_g \sim M^{0.22}$. The radial distributions of the dendrimers were developed identically in the PBC, irrespective of the core functionality. A gradual decrease in radial density resulted from the fact that the terminal branch ends are distributed all over the molecule, except for the core region.

Keywords: dendrimer, internal structure, molecular dynamics simulation, poly(benzyl ether).

Introduction

Dendrimers are three dimensional macromolecules consisting of a central core, an interior branch unit, and terminal end groups. They have a large number of symmetric branches with uniform segments, monodisperse molar masses, and regular tree-like topology, resulting from repetitive reaction sequences, such as the convergent[1] and divergent[2] synthetic approaches. Dendrimers have been extensively studied in both material sciences and biomedical areas, such as adhesives,[3] additives,[4] catalysts,[5] metal complex,[6] drug[7] and contrast agent carriers,[8] gene transfer agents,[9,10] and synthetic vaccines.[11]

Even though their structural features are unique in comparison to other commercial synthetic polymers, the geometric characteristics of dendrimers remain ongoing research topics within polymer science. There have been several controversial simulation results and experimental data as to the radial density distribution, the spatial distribution and location of the terminal end groups, and the maximum intrinsic viscosity. For instance, Lescanec and Muthukumar[12] published the molecular structures of a starburst model with maximum density near the core, and with terminal groups dispersed throughout the molecules. The small-angle neutron scattering (SANS) experiments[13] of poly(amidoamine) (PAMAM) dendrimer, and the nuclear magnetic resonance (NMR) relaxation time measurements[14] of poly(benzyl ether) (PBE) dendrimer in dilute solutions, on the other hand, fit the de Gennes and Hervet's model[15] of which most of the spacers are stretched and oriented away from the core. Naidoo and his co-workers have even investigated the potential use of organic and organochromic poly(benzylphenyl ether) (PBPE) as supporters for organometallic catalysts.[16] Recently, PAMAM in water solution[17] and poly(propylene imine) (PPI) dendrimer in melt[18] were simulated at the atomic level by using molecular dynamics (MD) simulation.

Molecular modeling techniques are widely used in polymer simulations as there has been great progress in the efficiency and availability of computational resources and methodologies.[19,20] Rotational isomeric state (RIS) approximation is the standard method for computing the conformational statistics of polymer chains. It is necessary to account for the enormous conformations accessible to a typical amorphous polymer. However, the RIS theory applies only to linear polymer chains whose statistical weight matrices are known beforehand, or are relatively easy to determine. Lately, the RIS Metropolis Monte Carlo (RMMC) method was developed to generate reliable torsional distributions for all kinds of polymers, including branched polymers in a relatively short time.[21] Dendrimers present particular challenges to molecular modeling of polymer materials due to their unique branched

*e-mail: hikim@cnu.ac.kr

structure and synthesis, as stated earlier. Dendrimers have been investigated using various theoretical models and simulation techniques, such as self-consistent field (SCF)[22] calculations, molecular mechanics (MM),[23] MD,[16-18,24,25] as well as Monte Carlo (MC) calculations.[26,27] MD or MC simulation, combined with MM is useful as a complementary protocol to generate different ensembles for the same target molecules.[28]

In this work, we performed MD simulations on the PBE dendrimer series with a different core type in bulk at 300 K. The RMMC method was used to construct the initial conformation of the PBE dendrimer in advance of the MD simulations. We attempted to obtain the detailed information on the structural features of the PBE dendrimers. The periodic boundary condition (PBC) was employed especially, in order to verify the effects of the introduction of branch points into the polymer structure. We calculated the radii of gyration and the fractal dimensions of the PBE dendrimers in order to investigate the relationship between the chain dimensions and generation number. The internal structure and morphology of the PBE dendrimers were monitored by the evaluation of the radial distribution functions, radial density, and frequency distribution of the branch ends.

Experimental

All simulations were performed using the Cerius^2 (Accelrys) software from Molecular Simulation Inc. on a Silicon Graphics O2 workstation comprising a R10000 processor. The polymer consistent force field (PCFF)[29-31] was used to calculate the potential energy surfaces in the RMMC and MD simulations. The nonbonded interaction energy (E_{nb}) was considered the sum of the atom pair interaction terms, calculated from the Coulombic force and Lennard-Jones 9-6 potential functions, as follows:

$$E_{nb} = \sum_{i>j} \frac{q_i q_j}{\varepsilon r_{ij}} + \sum_{i>j} \left[\frac{A_{ij}}{r_{ij}^9} - \frac{B_{ij}}{r_{ij}^6} \right]$$

where q_i is the partial charge on atom i, r_{ij} is the distance between the two atoms i and j, A_{ij} and B_{ij} are determined from the force field parameters for atoms i and j, and ε is the effective dielectric constant. In this simulation, ε was set to be 1.0.

Model. The PBE dendrimers were conventionally referred to monodendron and tridendron according to the core functionality employed in synthesis.[32] In this study, two different core types were used from 3,5-dihydroxybenzyl alcohol and 1,1,1-tris(4'-hydroxyphenyl)ethane, as shown in Figure 1. The various generations of the PBE dendrimers were designated by the use of the notation $[G\text{-}x]_n\text{-}f$, in which $[G\text{-}x]$ referred to generation number ($x = 0, 1, 2, 3, \cdots$), n was the number of dendritic fragments connected to the core, and f denoted the core moiety at the focal point.

Conformational Energy Surfaces. To find the conformational preference of the ether linkage, three torsion angels, ϕ, Ψ, and Ω were defined, as shown in Figure 2. The model dimer consisted of two 3,5-dihyroxybenzyl alcohol units connected via an ether linkage, and also represented the interior structure of the PBE dendrimer. The conformational energy surface was mapped as a function of the two adjacent torsional angles by energy minimization, with respect to the remaining geometric degree of freedom while the two torsion angles, ranged from -180° to 180° with the increment of 10°, were rigidly fixed.

Preparation of Amorphous Sample. To avoid hot spots caused by high potential energy, energy minimization was carried out with the convergence of 0.01 kcal/mol in advance of the RMMC simulations. The entire procedure of the RMMC calculation method is well explained elsewhere.[21] The bond length and angles were fixed and all rotatable single bonds were chosen to vary independently. The cut-off maximum bond value of 6.0 was used to include the interactions between the adjacent phenyl rings. Each PBE dendrimer molecule was arranged in a periodic cubic cell with a density of 1.0 according to both the torsional preferences obtained from the RMMC simulations, and the excluded volume interactions. The total energy of the simulation cell

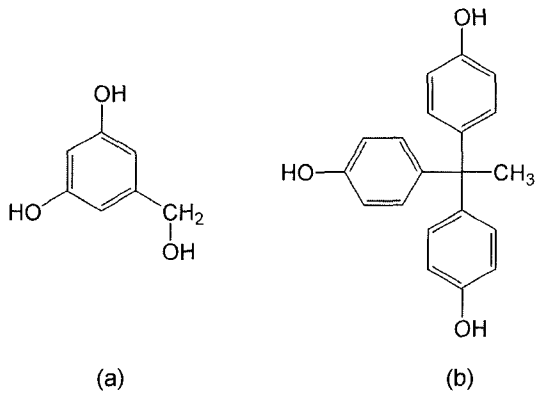

Figure 1. Core molecules of the PBE dendrimer: (a) 3,5-dihydroxybenzyl alcohol, and (b) 1,1,1-tris(4'-hydroxyphenyl)ethane.

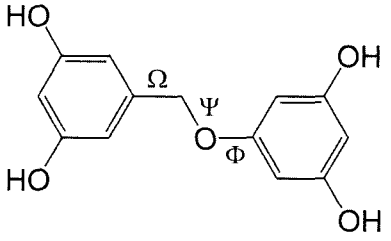

Figure 2. The model dimer of the PBE dendrimer used for conformational energy calculations.

was firstly minimized with all the cell parameters fixed, and then simulated annealing was carried out under 1 atm with the heating and cooling rate of 40 K per 1000 steps from 300 to 900 K. Each cycle of the annealing dynamics simulation was repeated 4 times until the total energy of the dendrimer system was converged. Figures 3 and 4 describe the typical structures of the PBE dendrimers initially generated and after the equilibrium process, respectively.

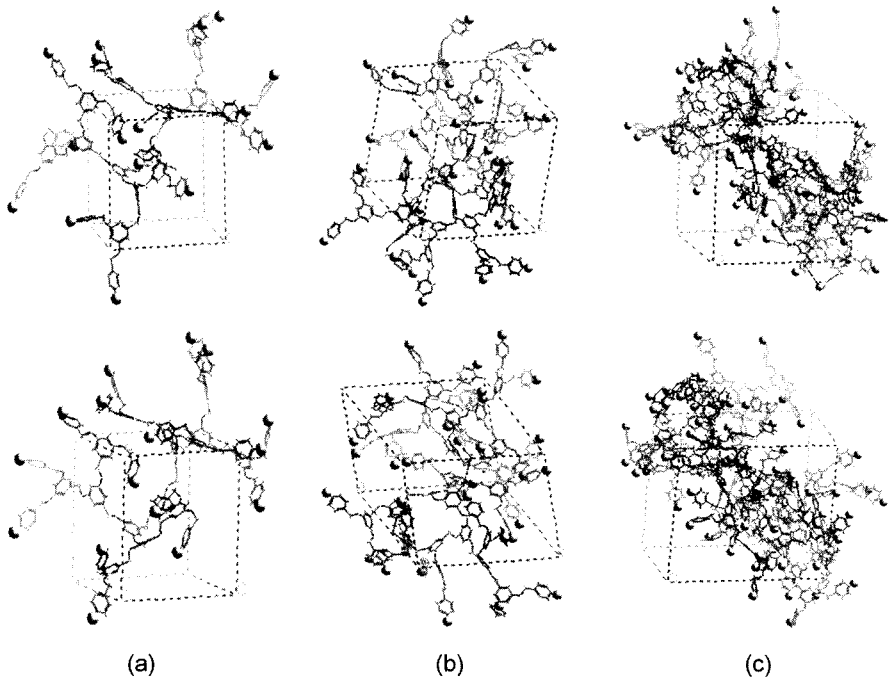

Figure 3. PBE dendrimer configurations obtained from the RMMC (above) and MD simulations (below): (a) $[G\text{-}4]_1$-OH, (b) $[G\text{-}5]_1$-OH, and (c) $[G\text{-}6]_1$-OH.

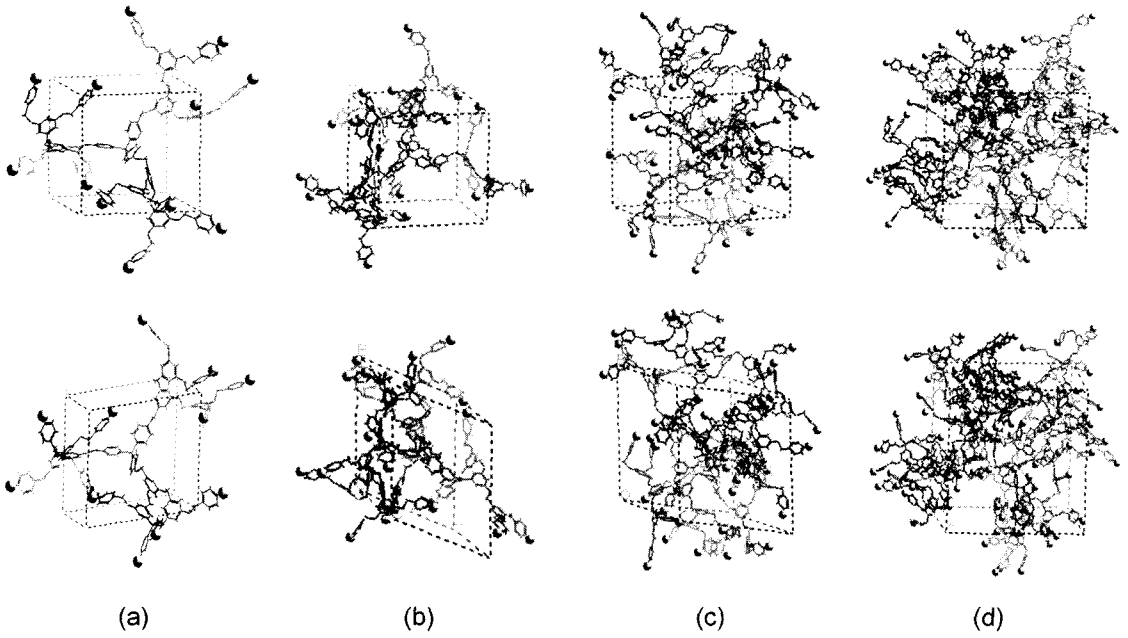

Figure 4. Tridendron PBE dendrimer configurations obtained from the RMMC (above) and MD simulations (below): (a) $[G\text{-}2]_3$-CH_3, (b) $[G\text{-}3]_3$-CH_3, (c) $[G\text{-}4]_3$-CH_3, and (d) $[G\text{-}5]_3$-CH_3.

Molecular Dynamics Simulations. After the annealing dynamics ran, the dendrimer system was fully equilibrated by the following MD simulation at 300 K under 1 atm for 300 ps. The Hoover thermoset with a coupling constant of 0.1 ps and the Parinello-Ramen method were used to control temperature and stresses, respectively, during the whole simulation time. The time step was normally chosen to be 1.0 fs, and the trajectory data were stored every 100 time unit. The spline switching method was applied to truncate the nonbonded forces on and off at 11 and 14 Å, respectively. The characteristics of the PBE structures, obtained from the MD simulations, were summarized in Table I. The average density of the PBE dendrimer did not change significantly as a function of generation number and molecular weight.

Results and Discussion

Conformational Energy Surfaces. To obtain the most probable conformation of the model dimer, the conformational energy surfaces were calculated for three defined torsions, ϕ, ψ, and Ω, as shown in Figure 2. Contour maps for the combination of two adjacent torsion angles provide useful information about the local chain structure.

Figure 5 shows the 2D contour of the conformational energy of the model dimer. In both contour maps, the lowest energy conformations were found in the region where the central torsional angle ψ was around $\pm 180°$. There were low energy regions around $\psi = \pm 180°$ and high energy regions around ψ=0°, irrespective of the values of the other torsion angles. In ϕ-ψ domain, it was most probable that the phenyl ring adjacent to the oxygen lay in the same plane with the ether linkage, because the two torsions assumed trans-trans state. For the torsion Ω, the lowest energy conformers were also found in the regions where $\Omega = \pm 110°$ and $\Omega = \pm 70°$ with a little larger tolerance. This showed that the phenyl ring of the benzyl group was more flexible than the phenyl ring adjacent to the ether oxygen. The terminal phenyl rings had a broad range of torsional preferences.

The probability distributions of the total torsion angles for each PBE dendrimer, calculated by the RMMC method are

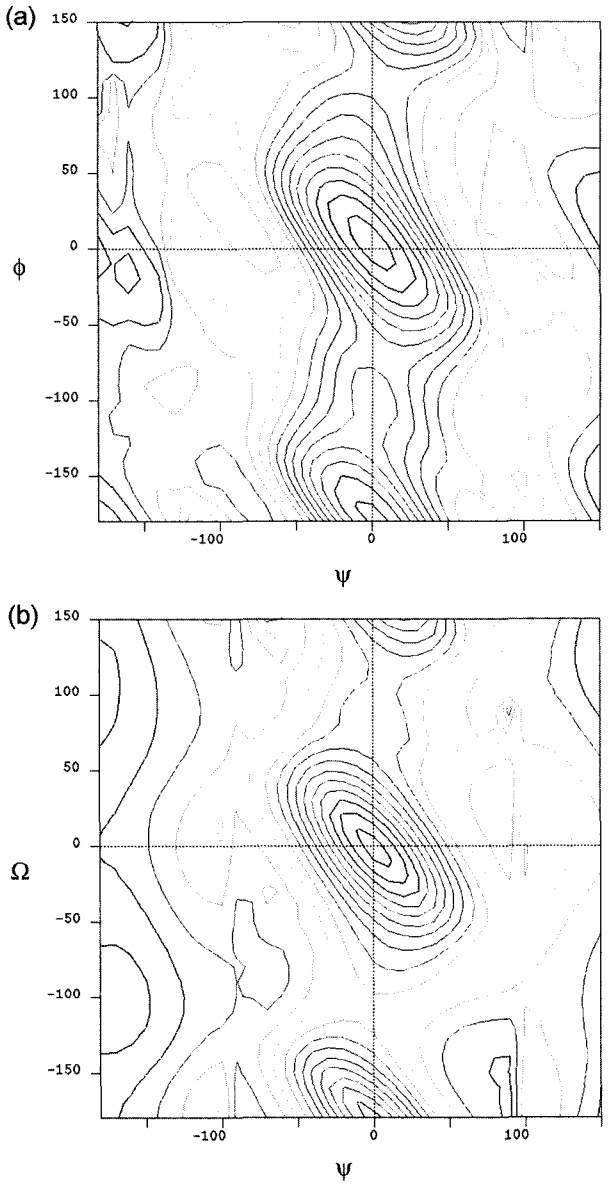

Figure 5. Conformational energy surfaces of the model dimer: (a) ψ vs. ϕ and (b) ψ vs. Ω.

Table I. Characteristics of the PBE Dendrimers

Core Type	Dendrimer	Density (g/cm^3)	R_g (Å)	Molar Mass	Number of Atoms	Number of Terminal Ends
Monodendron	$[G\text{-}4]_1$-OH	1.032	12.45	3,290	436	16
	$[G\text{-}5]_1$-OH	1.053	15.03	6,684	840	32
	$[G\text{-}6]_1$-OH	1.057	17.40	13,472	1,880	64
Tridendron	$[G\text{-}2]_3$-CH_3	1.049	12.83	2,487	332	12
	$[G\text{-}3]_3$-CH_3	1.062	14.77	5,034	668	24
	$[G\text{-}4]_3$-CH_3	1.068	17.48	10,128	1,340	48
	$[G\text{-}5]_3$-CH_3	1.075	19.78	20,316	2,684	96

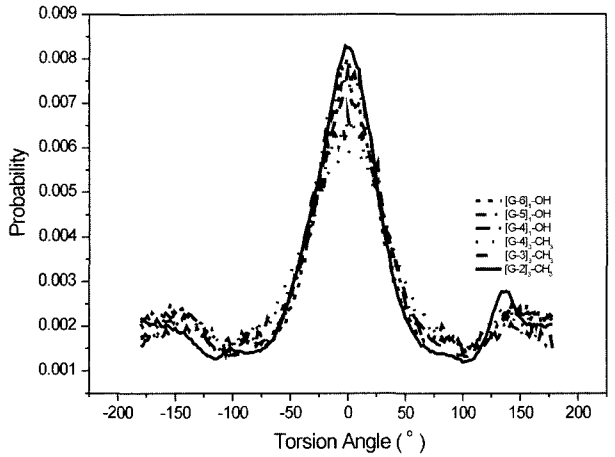

Figure 6. Torsion angle distributions obtained from the RMMC simulations at 300 K.

shown in Figure 6. There was an exclusive trans preference for each generation of PBE dendrimers. This preference was attributed to the interactions between the phenyl rings that were linked to the monomer units. The torsional distribution of the PBE dendrimers was consistent with the conformational energy maps for the model dimer, as shown in Figure 5.

The torsion angles involved in the ether linkage determine the conformational preference and chain dimension of the PBE dendrimer. The PBE dendrimer chains are known to be fully extended in a good solvent at room temperature.[33] In the bulk state at the same temperature, however, the PBE dendrimer adopted a less extended structure, allowed by the torsional preferences, as shown in Figures 7~9. As expected from the results of conformational energy contours, all torsions in the RMMC results were symmetric in relation to the trans position. The torsional space changed into the lower potential domain during the MD simulations after building the initial configurations. However, it was shown that the pattern of conformational changes in the PBE dendrimers differed, the more the core type varied. The main structural difference arose from the core size and its functionality. The symmetry did not change for all torsions of the tridendron PBE dendrimers. This was due to the fact that the larger core size and functionality of the tridendron PBE led to an increased distance between the dendrons, in order to minimize steric hindrances as compared to the monodendron.

For torsion ϕ, there was little difference among the three torsional distributions, except when a split occurred in the trans state of the tridendron PBE dendrimer. In Figure 7(c), the distribution about $\pm$ 180° was actually bimodal, with the fewer occurrences of exact trans geometry for the tridendron PBE. It was often found in the torsional distribution of chain branches introduced into the main chain where long range interactions were complex. Torsion ψ, which was initially all trans($\pm$ 180°), evolved to cluster the trans and the two or four gauche local minima. Figure 10 shows the change in the dimension and conformation of the monomer unit with the torsion ψ. These three conformations could be extracted from the MD trajectories with the populations, presented in Figure 8. The gauche local minima could be severely affected by the spatial arrangement of the segments

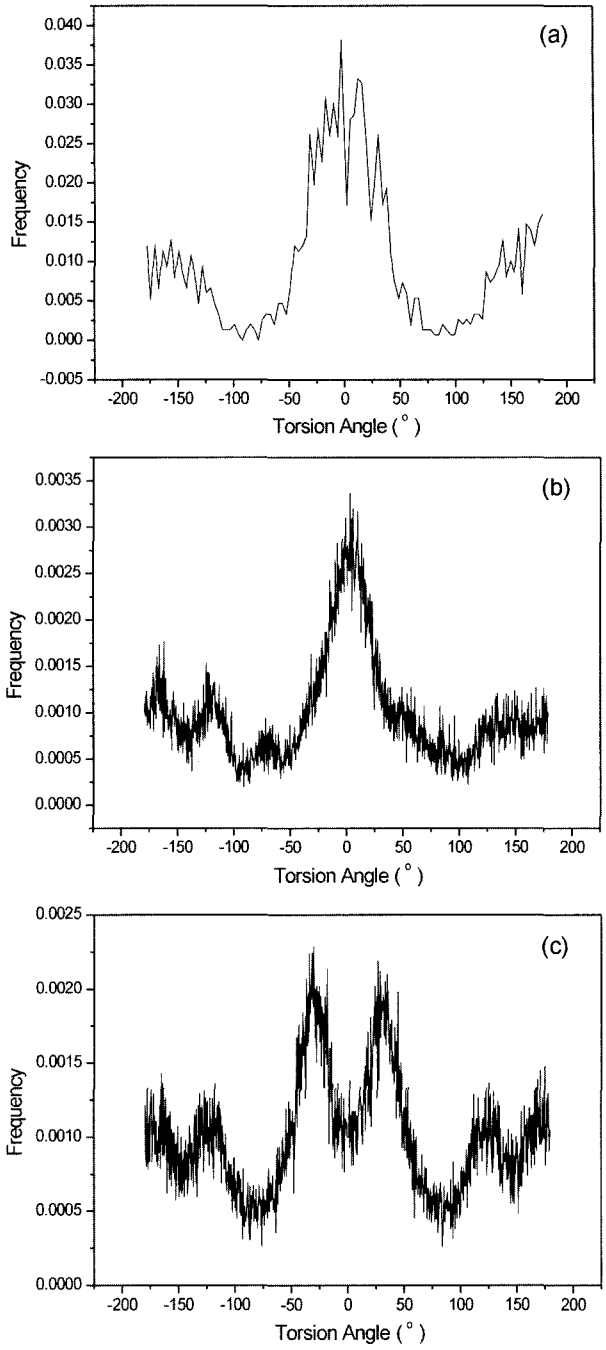

Figure 7. Distributions of torsion ϕ: (a) RMMC calculation, (b) [G-3]$_1$-OH MD simulation, and (c) [G-2]$_3$-CH_3 MD simuation.

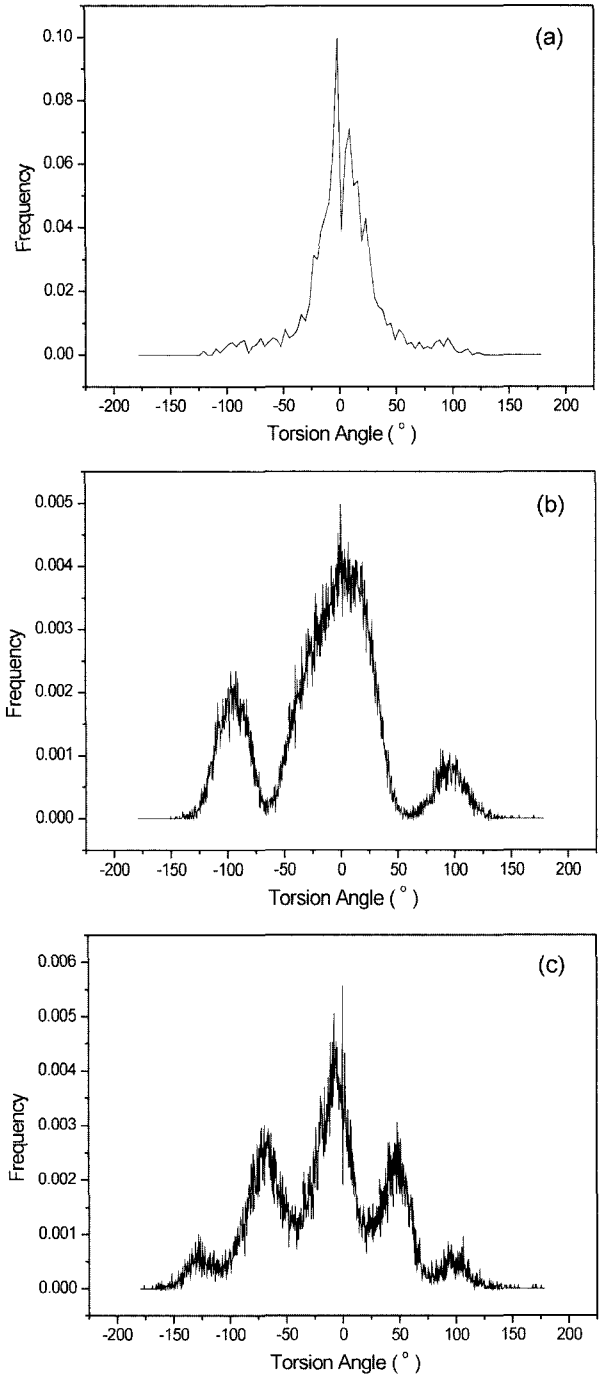

Figure 8. Distributions of torsion ψ: (a) RMMC calculation, (b) $[G\text{-}3]_1$-OH MD simulation, and (c) $[G\text{-}2]_3$-CH_3 MD simulation.

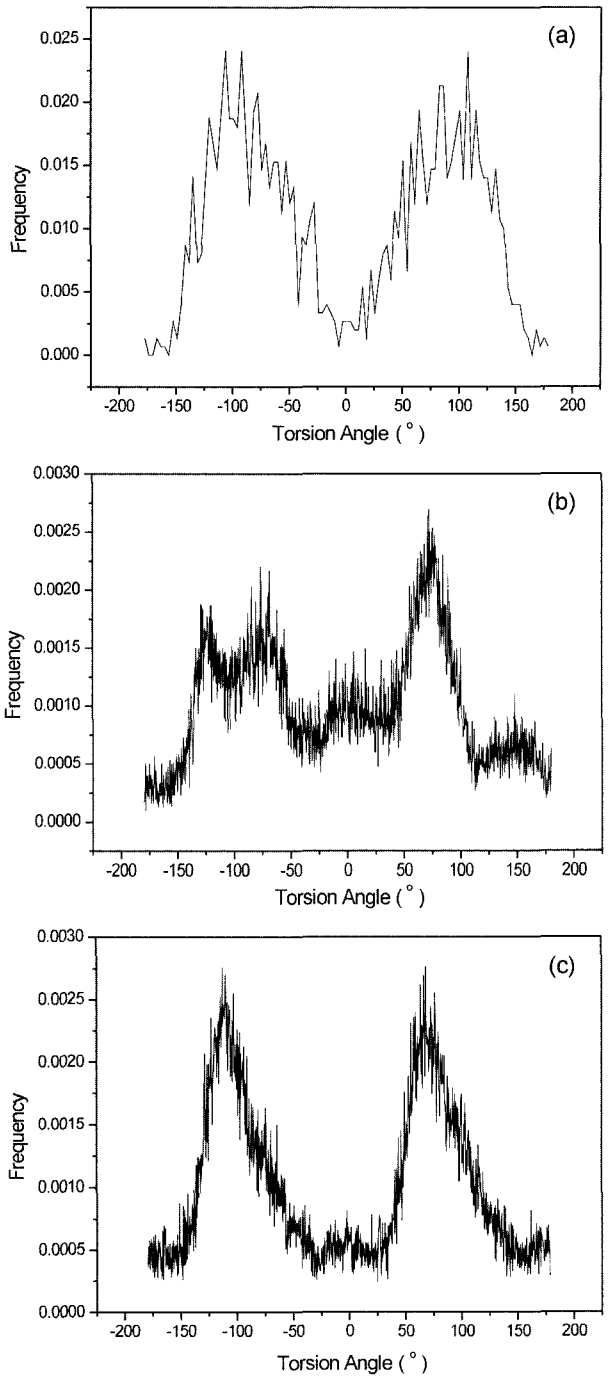

Figure 9. Distributions of torsion Ω: (a) RMMC calculation, (b) $[G\text{-}3]_1$-OH MD simulation, and (c) $[G\text{-}2]_3$-CH_3 MD simulation.

in the PBC. Therefore, biased gauche populations appeared at $\psi = \pm 80°$ for the monodendron PBE, and the new gauche states at $\psi = \pm 60°$ and $\psi = \pm 105°$ were allowed for the tridendron PBE.

Amorphous State. The PBE dendrimer configurations, obtained from the MD trajectories were in an amorphous state. It was confirmed by the radial distribution function (RDF) and structure factors(STF), as shown in Figure 11. The RDF was defined as the probability of finding any two atom pairs at a certain distance r, on the condition of the unit periodic cell volume. The total RDF meant the average distribution of interatomic vector lengths. The method of

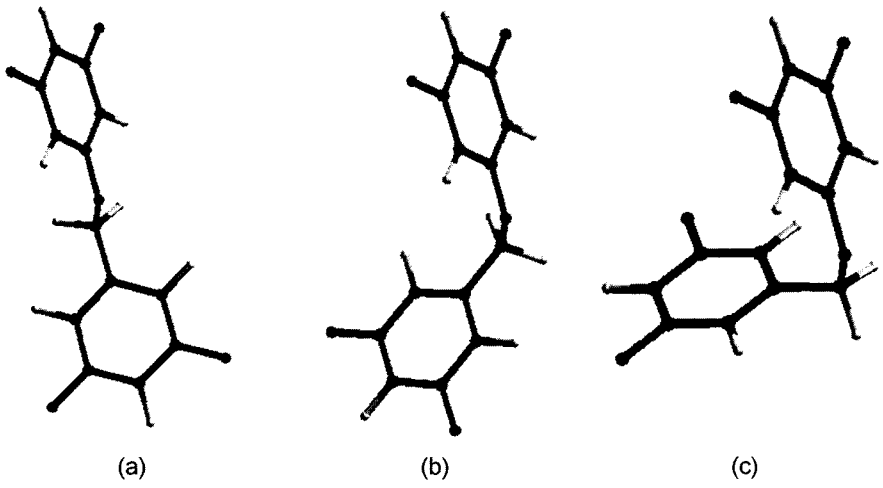

Figure 10. Probable conformations of the monomer unit in bulk at 300 K: (a) $\psi = \pm 180°$, (b) $\psi = \pm 120°$, and (c) $\psi = \pm 30°$.

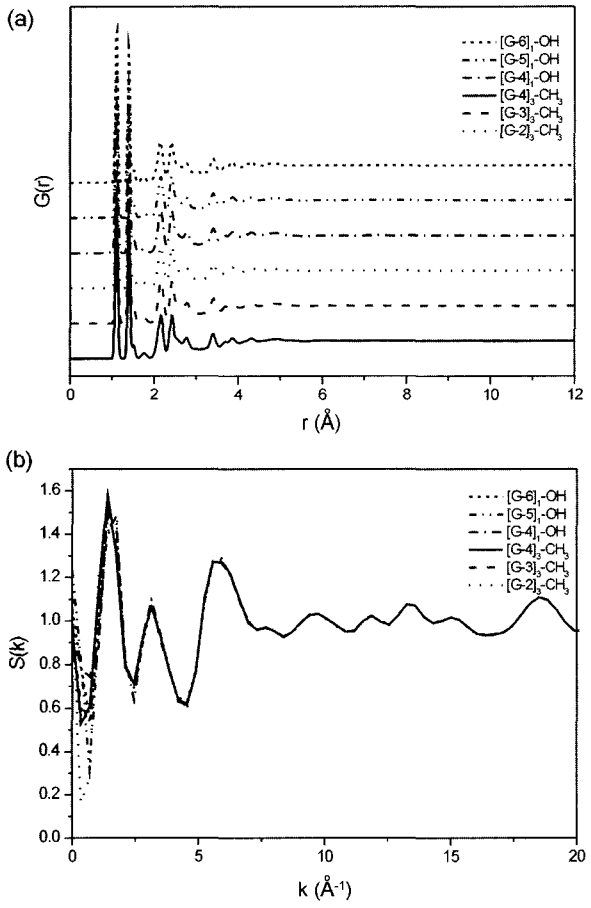

Figure 11. (a) Total radial distribution functions and (b) structure factors of each generation of PBE dendrimer series.

calculating RDF from the MD trajectory is discussed elsewhere.[34] The Fourier transforms of the total RDF were performed to calculate the STF for the PBE dendrimer. The total RDF and STF provided some useful information in revealing overall structural properties, such as packing, ordering, compressibility, and phase transitions, because they were directly compared with X-ray and neutron scattering data.

No long range order was observed at distances greater than 5 Å, which indicated that the PBE dendrimers at 300 K were amorphous glass. The peaks observed at distances less than 5 Å were assigned to the specific distances of any connected atom in the monomer unit. There was no difference in the total RDF, as the generation number and core functionality changed. These results implied that the core types did not have much influence on the overall chain configuration, due to its similarity to the monomer unit and small size of the focal points. It was clear that the uniform monomer segments in the chain branches could be generated randomly and independently from the core to the last generation.

Dimensions of the PBE Dendrimers. The average radii of gyration, R_g, were calculated as a function of the generation number, as presented in Table I. The radius of gyration is defined as

$$R_g = \sqrt{\frac{\sum_i m_i r_i^2}{\sum_i m_i}}$$

where r_i is the position vector of any atom i from the center of mass and m_i is the point mass of the atom i. Generally, the radii of gyration increased in accordance with the generation number for each core functionality. However, the increasing behavior of the R_g value between monodendron and tridendron PBE dendrimer was quite different due to different core functionalities. It was known that the monodendron

could provide a more free space in packing the PBC than the tridendron PBE did.

The molecular weight of the dendrimer increased exponentially to the generation number. To determine the relationship between the chain dimension and molecular weight for each functionality, a new equation, $<R_g> = AM^x$, was employed in Figure 12. Here, x was a reciprocal value of fractal dimension.[12,16,18,23] The solid lines and their slopes were obtained by the least squared fitting method for the equation. The value of x was 0.23 for the monodendron and 0.21 for the tridendron. Inverting this relation, these values corresponded to the fractal dimension of 4.34 and 4.76, respectively. This behavior resulted from the restriction of the highly branched structure of a single PBE dendrimer molecule in a 3D periodic cell. The branching nature of the PBE dendrimer became more developed in a periodic cell with the severe excluded volume interaction. The exponents were very close to the value of $x = 0.22$ in the scaling behavior of Lescanec and Muthukumar.[12] These results were also comparable to the Cayley tree, presented by Zimm and Stockmayer.[35] They showed that the radius of gyration was proportional to $M^{0.25}$. Generally, dendrimer melt is suitable to the study of scaling behavior because it produces conformations resembling the ones that result from the Θ condition, where the excluded volume interaction is remarkably reduced.[18] Many research groups presented the exponent value around 1/3 which indicated a space filling structure for the dendrimer in a confined radius.[18,23,25] In our study, the temperature was much lower than the condition in melt, where the dendrimer chains could be fully relaxed and extended.

Fractal Structure. We calculated the radial density for each PBE dendrimer to describe the internal structure. The radial density distribution is defined as follows:

$$\rho(r) = N(r)/4\pi r^2\, dr$$

We first determined the number of atoms, $N(r)$, within a spherical shell of radius r and thickness dr(0.2 Å), and then divided it by the volume of the shell. The normalized radial density distribution of the PBE dendrimer is shown in Figure 13. The radial density of the PBE dendrimer had its maximum

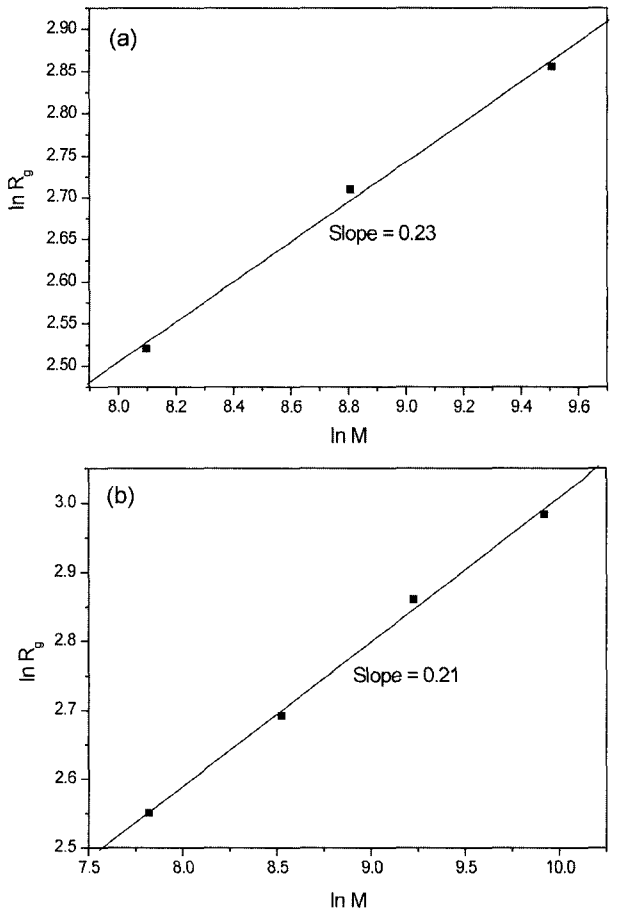

Figure 12. Radius of gyration of the PBE dendrimers as a function of molecular weight: (a) monodendron and (b) tridendron.

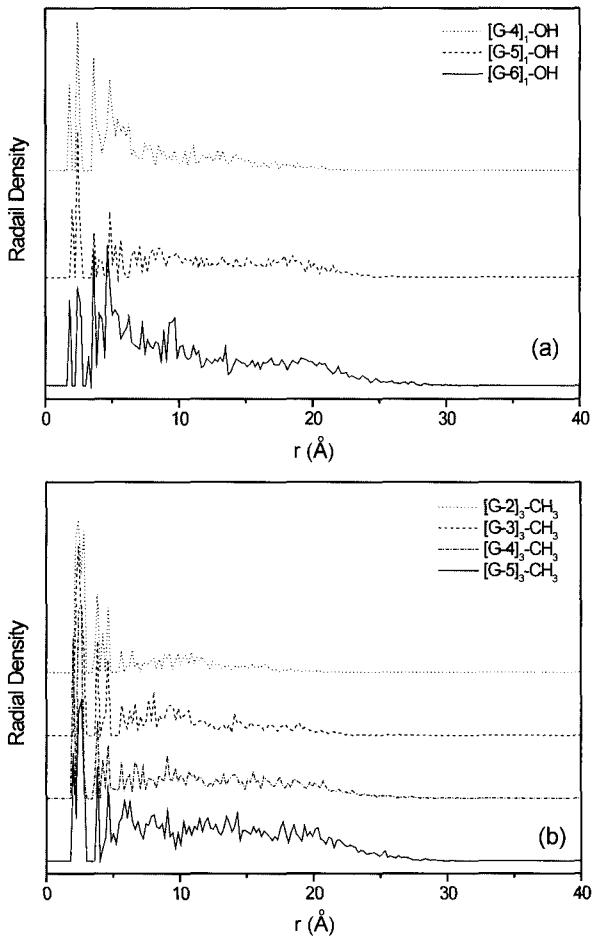

Figure 13. Normalized radial density distribution of the PBE dendrimers: (a) monodendron and (b) tridendron.

near the core, and monotonically decreased to the molecular periphery. The density profiles were consistent with the previous results of other simulation studies.[12,1517,23,25,26] The initial stage of radial density resulted from the atomic distance between the core and the first lying atoms in all generations. It was clear that the branch ends of the PBE dendrimers did not always lie on its surface.

We calculated the number of atoms ($W(r)$) within a sphere of radius (r) from the core. Here for simplicity and clarity, the reduced radius, r_{red}, was used to harmonize the different dimension and size of the PBE dendrimer. $W(r_{red})$ can be easily obtained from the radial density by using equation below.

$$W(r_{red}) = 4\pi\int_0^{r_{red}} r^2\rho(r)\, dr$$

Figure 14 showed that all the PBE dendrimers exhibited the same fractal structure, except for the chain dimensions. There was an identical pattern to configure the total atoms involved in the dendrimer for all generations. The radial distance between the core and any atoms in a PBE dendrimer

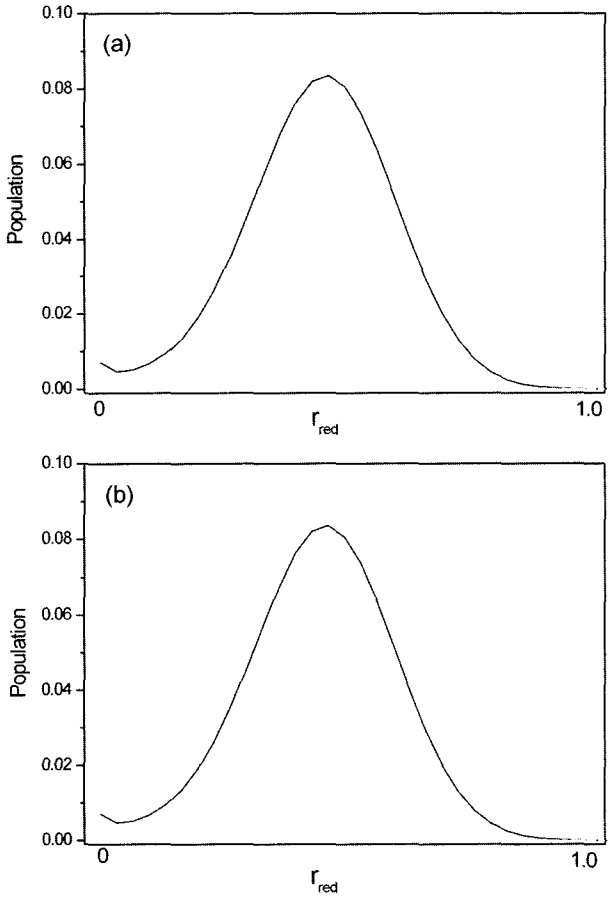

Figure 14. Frequency distribution of finding any atoms at r_{red} from the core: (a) monodendron and (b) tridendron.

followed the Gaussian distributions, as shown in Figure 14. The core functionality of the PBE dendrimer had little effect on the internal structure and morphology in bulk. The total number of atoms nearly doubled as the new generations were added to the terminal ends of the former chain branches. As the number of atoms increased in accordance with the generation number, a slightly different mode, occurred around the core at the lower generation, disappeared. Due to their large number of branch points and spherical shape, a slight increase in chain dimension resulted in the available volume which could accomodate the doubled number of whole atoms in the dendrimers.

Location of the Branch Terminals. Figure 15 shows the frequency distribution of the terminal ends of the PBE dendrimers. The location of the terminal ends differed as the core type and generation number varied. There was no regular pattern to locate the terminal end groups all over the shells which were introduced into the dendrimer structure when a new generation and its terminal ends were linked to the ends of the former generation. However, the terminal ends of the PBE dendrimer were prohibited in the core by the sterically unfavorable interactions when migrating closer than about 5 Å from the core. They were found even in the inner shell area. Therefore, the complex and different distribution for each generation of the PBE dendrimer was obtained from the MD trajectories. The terminal ends were distributed throughout the dendrimer molecule due to the conformational changes of the torsions ψ and Ω. It was also supported by $W(r)$, calculated from the radial density in the previous section.

Conclusions

We performed MD simulations of PBE dendrimer series in bulk at 300 K in order to obtain detailed information about the effects of the conformational changes of the monomer unit on the structural features. A PBE dendrimer in a PBC adopted less extended conformations because it was necessary to satisfy the acceptable nonbonded contacts and free volume requirements during the MD simulations. The torsional angles, involved in the ether linkages determined the conformational preference and chain dimension of the PBE dendrimers. The population of the torsion ϕ did little change during the simulation, but some extents of torsions ψ and Ω underwent transition to the gauche states. The pattern of conformational changes in the PBE dendrimers underwent great differences, the more the core functionality varied. However, the core type had little influence on the overall chain configuration, due to its similarity to the monomer unit and small size of the focal points. It was clear from the RDF results that the uniform monomer segments in the chain branches were generated randomly and independently from the core to the last generation.

The core functionality of the PBE dendrimer had little

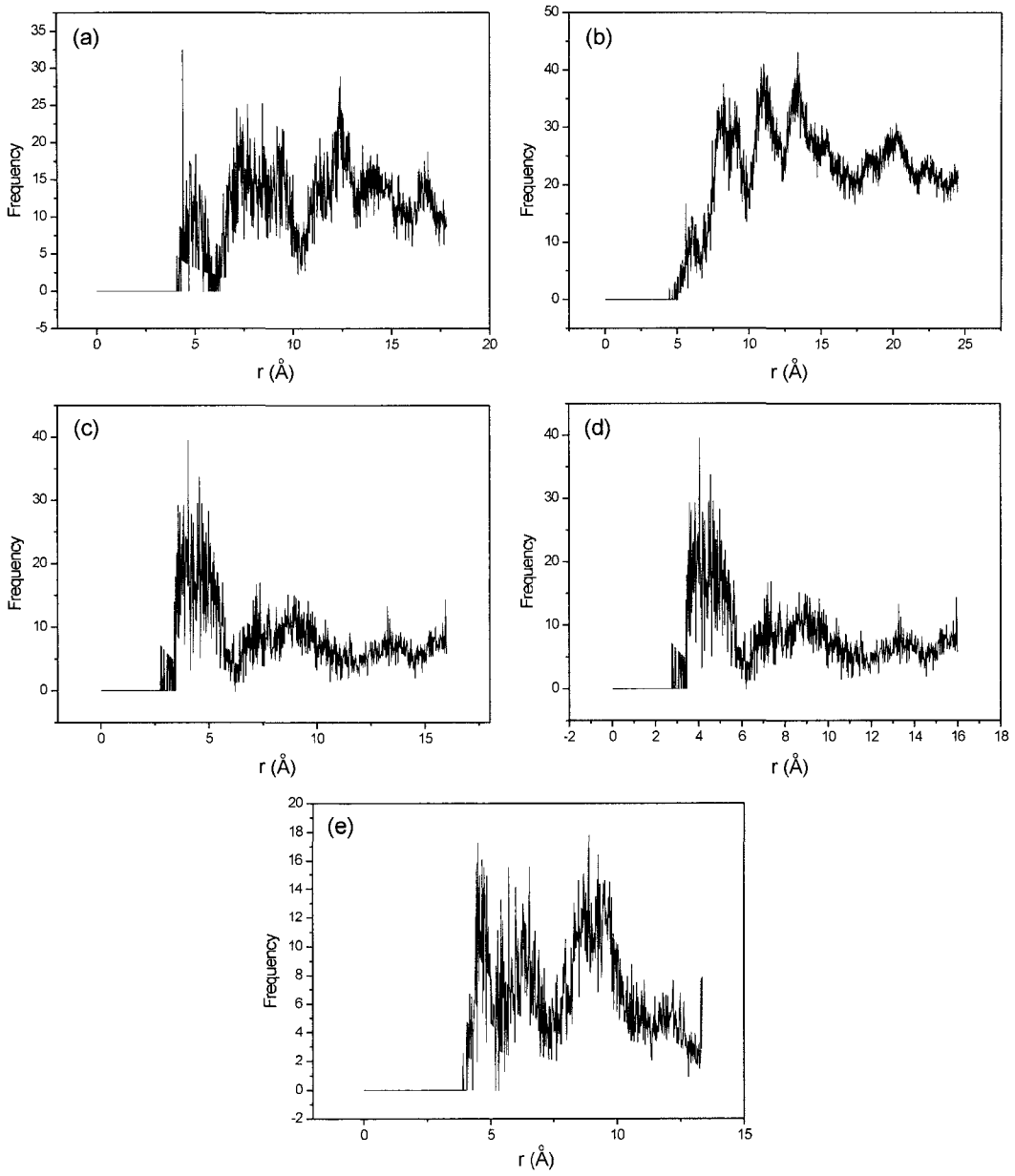

Figure 15. Frequency distribution of the radial distance between the core and branch ends: (a) $[G\text{-}4]_1$-OH, (b) $[G\text{-}5]_1$-OH, (c) $[G\text{-}2]_3$-CH_3, (d) $[G\text{-}3]_3$-CH_3, and (e) $[G\text{-}4]_3$-CH_3.

effect on the overall internal structure and morphology in bulk. The radial distance between the core and any atoms in a PBE dendrimer followed the Gaussian distribution. The terminal branch ends were distributed all throughout the molecule, except for the core region. The radial density exhibited a gradual decrease from the core toward the molecular periphery. The radius of gyration of the PBE glass agreed well with the scaling relation, $R_g \sim M^{0.22}$. This behavior resulted from both the highly branched structure of the PBE dendrimers and the periodic boundary condition employed to mimic the bulk glass state of the materials.

Acknowledgements. This work was supported to HIK for the 2001 overseas research dispatch by Chungnam National University.

References

(1) C. J. Hawker and J. M. J. Fretchet, *J Chem. Soc., Chem. Commun.*, **15**, 1010 (1990).
(2) D. A. Tomalia, H. Baker, J. Dewald, M. Hall, S. Martin, J. Roeck, J. Ryder, and P. Smith, *Polym. J.*, **17**, 117 (1985).
(3) D. A. Tomalia and L. R. Wilson, *U.S. Patent*, 4,713,975

(1987).
(4) F. M. Winnik, A. R. Davidson, and M. P. Breton, *U.S. Patent*, 5,120,361 (1992).
(5) D. A. Tomalia and P. R. Dvornic, *Nature*, **372**, 617 (1994).
(6) C. Kim, B. W. Koo, S. B. Lee, and C. K. Song, *Macromol. Res.*, **10**, 178 (2002).
(7) L. J. Twyman, A. E. Beezer, R. Esfand, M. J. Hardy, and J. C. Mitchell, *Tetrahedron Lett.*, **40**, 1743 (1999).
(8) E. C. Wiener, M. W. Brechbiel, H. Brothers, R. L. Magin, O. A. Gansow, D. A. Tomalia, and P. C. Lauterbur, *Magn. Reson. Med.*, **31**, 1 (1994).
(9) J. Haensler and F. C. Szoka, *Bioconjugate Chem.*, **4**, 372 (1993).
(10) M. F. Ottaviani, F. Furini, A. Casini, N. J. Turro, S. Jockusch, D. A. Tomalia, and L. Messori, *Macromolecules*, **33**, 7842 (2000).
(11) C. Rao and J. P. Tam, *J. Am. Chem. Soc.*, **116**, 975 (1994).
(12) R. L. Lescanec and M. Muthukumar, *Macromolecules*, **23**, 2280 (1990).
(13) M. Ballauff, *Top. Curr. Chem.*, **212**, 177 (2001).
(14) S. Hecht and J. M. J. Fretchet, *J. Am. Chem. Soc.*, **121**, 4084 (1999).
(15) P. G. de Gennes and H. Hervet, *J. Phys. Lett.*, **44**, L351 (1983).
(16) K. J. Naidoo, S. J. Hughes, and J. R. Moss, *Macromolecules*, **32**, 331 (1999).
(17) I. Lee, B. D. Athey, A. W. Wetzel, W. Meixner, and J. R. Baker, Jr., *Macromolecules*, **35**, 4510 (2002).
(18) N. Zacharopoulos and I. G. Economou, *Macromolecules*, **35**, 1814 (2002).
(19) S. H. Yang, J. S. Yang, and W. H. Jo, *Korea Polym. J.*, **8**, 224 (2000).
(20) S. S. Choi, *Korea Polym. J.*, **8**, 125 (2000).
(21) J. D. Honneycutt, *Compt. Theor. Polym. Sci.*, **8**, 1 (1998).
(22) D. Boris and M. Rubinstein, *Macromolecules*, **29**, 7251 (1996).
(23) M. Murat and G. S. Grest, *Macromolecules*, **29**, 1278 (1996).
(24) A. M. Naylor, N. A. Goddard, G. E. Kiefer, and D. A. Tomalia, *J. Am. Chem. Soc.*, **111**, 2339 (1989).
(25) M. L. Mansfield and L. I. Klushin, *Macromoleucles*, **26**, 4262 (1993).
(26) M. L. Mansfield, *Macromoleucles*, **33**, 8043 (2000).
(27) E. J. Wallace, D. M. A. Buzza, and D. J. Read, *Macromolecules*, **34**, 7140 (2001).
(28) W. L. Jorgenssen and J. Tirado-Ries, *J. Phys. Chem.*, **100**, 14508 (1996).
(29) H. Sun, *J. Comp. Chem.*, **15**, 752 (1994).
(30) D. Rigby, H. Sun, and B. E. Eichinger, *Polymer Int.*, **44**, 311 (1997).
(31) H. Sun and D. Rigby, *Spectrochimica Acta Part A*, **53**, 1301 (1997).
(32) T. H. Mourey, S. R. Turner, M. Rubinstein, J. M. J. Fretchet, C. J. Hawker, and K. L.Wooley, *Macromolecules*, **25**, 2401 (1992).
(33) S. de Backer, Y. Prinzie, W. Verheijen, M. Smet, K. Desmedt, W. Dehaen, and F. C. de Schryver, *J. Phys. Chem. A*, **102**, 5451 (1998).
(34) K. Jung, H. Kim, and J. Liu, *Korea Polym. J.*, **8**, 59 (2000).
(35) B. H. Zimm and W. H. Stockmayer, *J. Chem. Phys.*, **17**, 1301 (1949).